Title

HkRP3 Is a Microtubule-Binding Protein Regulating Lytic Granule Clustering and NK Cell Killing

Journal

The Journal of Immunology, 194(8)

ISSN

0022-1767

Authors

Ham, Hyoungjun
Huynh, Walter
Schoon, Renee A
et al.

Publication Date

2015-04-15

DOI

10.4049/jimmunol.1402897

Peer reviewed

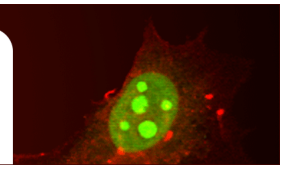

The Journal of Immunology

HkRP3 Is a Microtubule-Binding Protein Regulating Lytic Granule Clustering and NK Cell Killing

Hyoungjun Ham, Walter Huynh, Renee A. Schoon, Ronald D. Vale and Daniel D. Billadeau

J Immunol 2015; 194:3984-3996; Prepublished online 11 March 2015;
doi: 10.4049/jimmunol.1402897
http://www.jimmunol.org/content/194/8/3984

The Journal of Immunology is published twice each month by
The American Association of Immunologists, Inc.,
9650 Rockville Pike, Bethesda, MD 20814-3994.

Print ISSN: 0022-1767 Online ISSN: 1550-6606.

HkRP3 Is a Microtubule-Binding Protein Regulating Lytic Granule Clustering and NK Cell Killing

Hyoungjun Ham,* Walter Huynh,† Renee A. Schoon,*,‡ Ronald D. Vale,† and Daniel D. Billadeau*,‡

NK cells provide host defense by killing viral-infected and cancerous cells through the secretion of preformed lytic granules. Polarization of the lytic granules toward the target cell is dependent on an intact microtubule (MT) network as well as MT motors. We have recently shown that DOCK8, a gene mutated in a primary immunodeficiency syndrome, is involved in NK cell killing in part through its effects on MT organizing center (MTOC) polarization. In this study, we identified Hook-related protein 3 (HkRP3) as a novel DOCK8- and MT-binding protein. We further show that HkRP3 is present in lytic granule fractions and interacts with the dynein motor complex and MTs. Significantly, depletion of HkPR3 impaired NK cell cytotoxicity, which could be attributed to a defect in not only MTOC polarity, but also impaired clustering of lytic granules around the MTOC. Our results demonstrate an important role for HkRP3 in regulating the clustering of lytic granules and MTOC repositioning during the development of NK cell–mediated killing. ***The Journal of Immunology*****, 2015, 194: 3984–3996.**

Natural killer cells are lymphocytes of the innate immune system that play an essential role in the clearance of viral-infected cells and cancer cells (1, 2). Various germline-encoded activating and inhibitory receptors are expressed on the surface of NK cells, and current knowledge suggests that integrated signals from these receptors enable NK cells to distinguish unhealthy "non-self" cells from healthy "self" cells, thereby regulating NK cell activation (3). The main consequence of NK cell activation is the killing of bound target cells via the directed secretion of preformed secretory lysosomes called lytic granules.

Multiple molecular features are observed during NK cell–mediated cytotoxicity. For example, after the initial adhesion to target cells, NK activating receptors, as well as integrins and F-actin, accumulate at the center of the NK cell/target interface, forming the cytotoxic synapse (CS) (3–5). Concurrent with this, lytic granules are rapidly clustered around the microtubule organizing center (MTOC) by the dynein/dynactin minus-end-directed MT motor complex that constitutively associates with lytic granules (6). Subsequently, the MTOC is polarized toward the CS to allow directed secretion of the lytic granule contents toward the bound target cell. Therefore, delivery of lytic granules is dependent on tight regulation of both the MT network as well as its associated motor proteins. However, the detailed mechanism for this regulation remains elusive.

Dedicator of cytokinesis 8 (DOCK8) deficiency is a primary immunodeficiency that affects NK cell cytotoxicity (3, 7, 8). This disease is inherited in an autosomal recessive manner, and the main clinical symptoms are elevated serum IgE levels, recurrent infections in the lung and skin, and severe allergies (9–11). Others and we have previously shown that DOCK8 is a CDC42 guanine nucleotide exchange factor and DOCK8-deficient/-depleted human NK cells show defective cytotoxic activity (7, 8, 12). At the molecular level, DOCK8 deficiency resulted in defective accumulation of F-actin at the CS, impaired integrin-mediated adhesion, and MTOC polarization (7, 8, 13). Using mass spectrometry, we previously found that DOCK8 interacted with WASP and talin, two key regulators of F-actin generation and integrin affinity maturation, respectively (8). Significantly, depletion of DOCK8 led to a reduced recruitment of both proteins to the CS, which may account in part for the defects in F-actin accumulation and integrin-mediated adhesion. Mechanisms by which DOCK8 contributes to MTOC polarization are not known.

In the present study, we characterize a protein known as Hook-related protein 3 (HkRP3, also called CCDC88B, FLJ00354, or Gipie) as a novel DOCK8-interacting protein. HkRP3 is one of three members of the Girdin protein family, which includes Girdin and Daple (14, 15). All Girdin family members contain an N-terminal region with sequence homology to the microtubule-binding domain of Hook proteins. Additionally, all members contain a long coiled-coil region at their center and a variable unique region at the C terminus. Previously, Matsushita and colleagues (15) reported that HkRP3 is an important regulator of endoplasmic reticulum (ER) stress response in endothelial cells via its interaction with 78-kDa glucose-regulated protein (GRP78). However, little is known about cellular roles of HkRP3 in hematopoietic cells, where HkRP3 has been suggested to be preferentially expressed based on expressed sequence tag databases (14, 15). In the present study, we demonstrate that HkRP3 mediates NK cell cytotoxicity in part through its ability to regulate lytic granule

*Department of Immunology, Mayo Graduate School, College of Medicine, Mayo Clinic, Rochester, MN 55905; †Department of Cellular and Molecular Pharmacology, Howard Hughes Medical Institute, University of California San Francisco, San Francisco, CA 94158; and ‡Division of Oncology Research, Schulze Center for Novel Therapeutics, College of Medicine, Mayo Clinic, Rochester, MN 55905

Received for publication November 17, 2014. Accepted for publication February 5, 2015.

This work was supported by the Mayo Foundation and National Institutes of Health Grant R56-AI112538 (to D.D.B.). H.H. was supported by the Mayo Graduate School. The Gene Analysis Core Shared Resource is supported in part by Mayo Clinic Comprehensive Cancer Center Support Grant P30CA15083.

Address correspondence and reprint requests to Dr. Daniel D. Billadeau, Division of Oncology Research, Schulze Center for Novel Therapeutics, College of Medicine, Mayo Clinic, 200 First Street SW, Rochester, MN 55905. E-mail address: billadeau.daniel@mayo.edu

The online version of this article contains supplemental material.

Abbreviations used in this article: CMAC, 7-amino-4-chloromethylcoumarin; CS, cytotoxic synapse; DIC, dynein intermediate chain; DOCK8, dedicator of cytokinesis 8; ER, endoplasmic reticulum; GRP78, 78-kDa glucose-regulated protein; HkRP3, Hook-related protein 3; MBP, maltose-binding protein; MT, microtubule; MTOC, microtubule organizing center; PEI, polyethylenimine; PLL, poly-L-lysine; RILP, Rab-interacting lysosomal protein; siRNA, small interfering RNA.

www.jimmunol.org/cgi/doi/10.4049/jimmunol.1402897

clustering and MTOC polarization. We further show that HkRP3 directly binds to MTs via its unique region at the C terminus and also interacts with the dynein/dynactin motor complex, which transports lytic granules along MTs. Taken together, our results provide a novel cellular function for HkRP3 during the development of NK cell cytotoxicity.

Materials and Methods

Cells, reagents, and Abs

YTS cells were obtained from Dr. E. Long (National Institutes of Health, Bethesda, MD), NKL cells were from Dr. M. Robertson (Indiana University Cancer Center, Indianapolis, IN), and primary human NK cells were cloned and passaged as previously described (16). Two separate rabbit polyclonal antisera to HkRP3 (National Center for Biotechnology Information no. NP_115627.6) were obtained by immunizing rabbits with GST-conjugated HkRP3 aa 821–927 [anti-HkRP3(1)] and aa 1387–1476 [anti-HkRP3(2)] (Cocalico Biologicals, Reamstown, PA). Anti-HkRP3(1) was used for immunoblot and immunoprecipitation and anti-HkRP3(2) was used for immunofluorescence assays in this study. Polyclonal rabbit anti-serum for DOCK8 was previously described (8). Abs for α-tubulin, γ-tubulin, and FLAG (clone M2) were purchased from Sigma-Aldrich, and Abs for maltose-binding protein (MBP; Immunology Consultants Laboratory), $p150^{Glued}$ (BD Biosciences), dynein intermediate chain (DIC; Millipore), β-actin (Cell Signaling Technology), and granzyme B (Santa Cruz Biotechnology) were purchased as indicated. Nocodazole was purchased from Selleckchem.com.

Small interfering RNA constructs and nucleofection

Small interfering RNA (siRNA) duplexes were obtained from Dharmacon: siControl, 5′-UUCUCCGAACGUGUCACGU-3′; siHkRP3 no. 1, 5′-GCAUGAGAAUAAAGCUGAA-3′; siHkRP3 no. 2, 5′-GGCAGGAGUUGGCAAGAGA-3′; and siDOCK8, 5′-GGAGAUUAUUUGUGAACUU-3′. Nucleofection of siRNA oligonucleotides into YTS, NKL, and NK clones was performed as previously described (17, 18).

Plasmids and transfection

The pCI2.FLAG.YFP.DOCK8 construct was previously described (8). Full-length HkRP3 (National Center for Biotechnology Information no. NP_115627.6) was cloned into the pCI2 plasmid in-frame with FLAG.YFP or EE. All constructs were sequenced validated in the Gene Analysis Core shared resource of the Mayo Clinic Comprehensive Cancer Center. HEK293T cells were transfected using polyethylenimine (PEI; Polysciences). HEK293T cells were prepared in 10-cm cell culture plates at 70–80% confluency on the day of transfection. Six micrograms total plasmid DNA was diluted in 400 μl OptiMEM media (Life Technologies), and 72 μl PEI dissolved in water (2 mg/ml) was added. After 15 min of incubation at room temperature, the volume of medium in the cell culture plate was adjusted to 5 ml, and the mixture was added to HEK293T cells dropwise. Cells with PEI mixture were incubated at 37 ˚C for 90 min, and the medium was then changed with fresh growth medium. Experiments were performed 48 h after transfection.

Immunoprecipitation and GST pull-down assays

For immunoprecipitation, cells were lysed in Nonidet P-40 lysis buffer (25 mM HEPES [pH 7.9], 25 mM NaCl, 0.5% Nonidet P-40, 1 mM EDTA, 0.5 mM $CaCl_2$, 1 mM PMSF, 10 μg/ml leupeptin, and 5 μg/ml aprotinin), and immunoprecipitations were performed as previously described (19). GST fusion protein pull-downs were performed as previously described (8). To examine direct interactions, 30 μg GST fusion protein bound to glutathione-agarose slurry was incubated with 30 μg MBP fusion protein for 3 h at 4˚C.

Microtubule co-pelleting assay

Both in vitro microtubule assembly and microtubule co-pelleting assays were performed according to the manufacturer's instruction (Cytoskeleton). Fusion proteins were spun at 120,000 × *g* for 40 min at 4˚C, and the supernatant was collected before the assay. Various concentrations of microtubules were incubated with 0.5 μM fusion proteins at room temperature for 30 min. Then, samples were spun at 100,000 × *g* for 40 min at room temperature, and supernatants and pellets were collected for SDS/PAGE analysis. Depending on the m.w. of fusion proteins used, tubulin and fusion proteins were visualized either by Coomassie blue staining or by immunoblotting.

Cytotoxicity assay

The ^{51}Cr-release assays were performed as previously described (16). All LU values in this study were obtained by calculating the required number of NK cells to kill 20% of target cells.

Conjugate assay

YTS cells were labeled for 30 min at 37˚C with 2.5 μM CellTracker Violet BMQC (Invitrogen), and 721.221 target cells were labeled for 30 min at 37˚C with 0.75 μM CFSE (eBioscience). Labeled cells were then washed and resuspended at 1.6×10^6 cells/ml. Cells (250 μl of each) were mixed together, centrifuged at 200 rpm for 5 min, and allowed to incubate at 37˚C for up to 15 min before fixation by adding 4% paraformaldehyde in PBS. Conjugate formation was assessed using two-color flow cytometry and analyzed as the percentage of target-bound NK cells ($violet^+green^+$) over total NK cells ($violet^+$).

Microscopy

For microscopy of single siRNA-transfected YTS cells, 1.6×10^5 cells were plated on poly-L-lysine (PLL)–coated coverslips for 10 min at 37˚C. For microscopy of conjugated YTS cells with target cells, 250 μl (1.6×10^6 cells/ml in serum-free RPMI 1640 medium) of untransfected or siRNA-transfected YTS cells (72 h after transfection) cells were mixed with an equal volume of 7-amino-4-chloromethylcoumarin (CMAC; Invitrogen)–stained 721.221 target cells (1.6×10^6 cells/ml in serum-free RPMI 1640 medium) and centrifuged together at 200 rpm for 5 min. In the case of time-course experiments, cells were incubated at 37˚C for 1, 5, 15, and 25 min, resuspended, and incubated on PLL-coated coverslips for 5 min at 37˚C. In the case of single time point experiments, the lightly pelleted cells were incubated at 37˚C for 15 min, resuspended, and allowed to adhere to PLL-coated coverslips for 10 min at 37˚C. For stimulation of YTS cells with Ab-coated coverslips, Ab-coated coverslips were prepared as previously described using anti-CD28 Ab (BD Biosciences) and anti-CD45 Ab (BD Biosciences) (17). YTS cells were then dropped on coverslips and incubated for 25 min at 37˚C.

Cells were fixed with either methanol or 4% paraformaldehyde in PBS and stained with specific Abs (anti-HkRP3, anti–LFA-1 [clone MHM23], anti-perforin [BD Biosciences], anti–α-tubulin [Sigma-Aldrich], anti–γ-tubulin [Sigma-Aldrich], anti-$p150^{Glued}$ [BD Biosciences], and anti-DIC [Millipore]). Secondary reagents included FITC-, tetramethylrhodamine-, Alexa Fluor 568–, or Alexa Fluor 488–labeled goat anti-mouse IgG, or goat anti-rabbit IgG (Invitrogen). F-actin was visualized with Alexa Fluor 488–phalloidin or rhodamine-phalloidin (Invitrogen). Coverslips were mounted on glass slides using SlowFade reagent (Invitrogen) and examined on microscopes at room temperature. Most of the prepared slides were examined with a Plan-Apochromat ×100/1.46 numerical aperture oil immersion objective equipped on an LSM 710 laser-scanning confocal microscope (Carl Zeiss). Additional slides were examined with a Plan-Apochromat ×100/1.40 numerical aperture oil immersion objective on an Axiovert 200 microscope (Carl Zeiss) equipped with a digital camera (AxioCam HRC; Carl Zeiss). Images were captured with either the AxioVision or LSM software packages (Carl Zeiss).

Image analysis

ImageJ software (version 1.45s; National Institutes of Health) was used for processing microscopic images in this study. To calculate the mean fluorescence intensity of HkRP3 within a cell, whole-cell areas enclosed by cortical actin (visualized with fluorescently labeled phalloidin) and the sum intensity of HkRP3 within the region were measured. Quantification of fluorescence intensity for LFA-1 at the YTS/721.221 interface was performed as previously described (8). Images containing a total of 30 conjugates were taken for each condition (10 conjugates/experiment; three independent experiments) and analyzed. For quantification of mean distance of lytic granules to the MTOC and distance between the MTOC and the CS, each image was taken after setting the focal plane to visualize γ-tubulin (representing MTOC) of a YTS cell. To calculate the mean distance of lytic granules from the MTOC, we first obtained *x*- and *y*-coordinates of each lytic granule (visualized by perforin stain) in a YTS cell as well as those of γ-tubulin. Then, we weighted each granule to MTOC distance by the granule area before calculating the mean MTOC distance; this method allowed for quantification of clustered lytic granules, which could appear as a single granule in many cases and potentially bias the mean granule to MTOC distance as previously described (6). The assumption for this area-weighted mean distance is that sizes of lytic granules in a specific YTS cell are the same, so the minimum granule area detected in a YTS cell represents a single lytic granule. Taking this as-

sumption, the mean distance between lytic granules to MTOC was calculated using Eq. 1:

$$\text{Total granule area (TGA)} = \sum_{i=1}^{n} A_i$$

(where A_i indicates the area of an individual lytic granule and n refers to the total number of lytic granules)

$$\text{Average distance of lytic granules from MTOC} = \sum_{i=1}^{n} \frac{A_i}{TGA} \times \sqrt{(x - x_i)^2 + (y - y_i)^2} \quad (1)$$

where x and y represent coordinates of the MTOC centroid, x_i and y_i are coordinates of an individual lytic granule centroid, A_i is the area of an individual lytic granule, and n represents the total number of lytic granules. The distance between the MTOC and the CS was calculated after obtaining x- and y-coordinates of the MTOC centroid as well as those of the center of the YTS/target interface.

Intracellular staining of perforin and granzyme B

Intracellular perforin and granzyme B levels were examined as previously described using FITC-perforin (BD Biosciences) and FITC–granzyme B (BD Biosciences) (20).

Lysosome fractionation

Preparation of the crude lysosome fraction was performed as previously described (21). YTS cells (40×10^6) were resuspended with 500 μl 0.25 M sucrose in 10 mM Tris (pH 7.4) and homogenized with a dounce tissue homogenizer. The homogenate was spun at $600 \times g$ for 5 min at 4˚C and the supernatant (postnuclear lysate) was collected and spun again at $12{,}000 \times g$ for 10 min at 4˚C. The supernatant was then collected and $CaCl_2$ was added to the supernatant to a final concentration of 8 mM and mixed well. The mixture was then spun at 13,000 rpm for 15 min at 4˚C, and the supernatant was collected as the non–lysosomal fraction. Pellets were washed once with 150 mM KCl in 10 mM Tris (pH 7.4), resuspended with 80 μl 150 mM KCl in 10 mM Tris (pH 7.4), and saved as the crude lysosomal fraction (CLF).

Cell stimulation

In experiments involving cell surface receptor (NKG2D and 2B4) cross-linking, 15×10^6 NKL cells were prepared for each stimulation condition. Anti-NKG2D (R&D Systems) and anti-2B4 (clone C1.7) were added at a final concentration of 5 μg/ml to 150 μl cell suspension and incubated together for 10 min on ice. Washed cells were then incubated with goat anti-mouse IgG $F(ab')_2$ (Cappel) at 37˚C for the indicated periods of time.

Statistical analysis

Statistical analyses of percentage LUs (Fig. 2B, 2C) were performed using a one-sample t test with a hypothetical value of 100. For statistical analyses of "percentage of incidences" (*bottom panels* of Figs. 4B, 4C, 5B, 5C), a proportion z test was performed. All other statistical analyses in this study were performed using a two-tailed Student t test.

Results

HkRP3 interacts with DOCK8 and exists as an oligomer

Our prior mass spectrometry analysis aimed at identifying DOCK8-interacting partners detected WASP and talin as well as several additional proteins (8), including HkPR3, which is largely uncharacterized. According to an expressed sequence tag database (14), HkRP3 is preferentially expressed in hematopoietic cells and its expression in myeloid and monocytoid leukemic cell lines as well as in endothelial cells was confirmed previously (15). However, its expression has not been examined in human NK cells. Therefore, we prepared two human NK cell lines, NKL and YTS, and primary human NK cells along with several other cell lines and examined HkRP3 expression at the protein level (Fig. 1A). HkRP3 expression was detected in all human NK cells as well as two other human hematopoietic cell lines (Jurkat T cells and 721.221 B cells). Consistent with previous findings, we were not able to detect HkRP3 in HEK293T or HeLa cells (15). Unexpectedly, we did not detect HkRP3 in the human myelogenous leukemia cell line K562.

Because HkRP3 was identified as a potential DOCK8-interacting protein, we first determined whether they interacted by transfecting HEK293T cells with plasmids encoding FLAG.YFP or FLAG.YFP-DOCK8 along with EE-only or EE-tagged HkRP3. Consistent with our mass spectrometry results, we observed that HkRP3 coimmunoprecipitated with DOCK8 (Fig. 1B). Importantly, we were also able to confirm that endogenous DOCK8 and HkRP3 coimmunoprecipitated with each other in YTS cells (Fig. 1C).

Girdin was suggested to form an oligomer mediated by its N-terminal region (14, 22). The region responsible for oligomer formation is shared among the members of the Girdin family, suggesting that HkRP3 might also exist as an oligomer. To test this possibility, we first transfected HEK293T cells with plasmids encoding FLAG.YFP or FLAG.YFP-HkRP3 along with EE-only or EE-tagged HkRP3 and performed immunoprecipitation using anti-EE Ab. We consistently found that EE-tagged HkRP3 coimmunoprecipitated together with FLAG-tagged HkRP3, suggesting that it can interact with itself (Fig. 1D). We next tested whether the interaction was in fact mediated by the N-terminal region of HkRP3 by incubating either GST- or MBP-fused N-terminal HkRP3 proteins (Fig. 1E) and performing a GST pull-down assay (Fig. 1F). Significantly, the GST-fused first half of HkRP3 successfully pulled down the same region of HkRP3 fused with MBP. Although our findings do not represent the endogenous oligomerization state of HkRP3, these data indicate that HkRP3 minimally forms a homodimer similar to Girdin and interacts with DOCK8.

HkRP3 mediates NK cell cytotoxicity

To determine whether HkRP3 is involved in NK cell cytotoxicity, we compared the cytotoxic activity of YTS cells after depletion of HkRP3 using two different siRNA oligonucleotide duplexes. Seventy-two hours after transfection, we examined natural cytotoxicity using the 721.221 B lymphoblastoid cell line as tumor target cells (Fig. 2A). Consistent with our previous findings, DOCK8-depleted YTS cells showed less cytotoxicity compared with control siRNA-transfected cells (8). Surprisingly, both HkRP3-suppressed YTS cells showed strong defects in cytotoxic activity similar to that of DOCK8 (Fig. 2A, *left* and *center panels*). Relative cytotoxicity (LUs) was also diminished in the HkRP3-depleted cells compared with that of the control group (Fig. 2A, *right panel*). We also observed a similar decrease in cytotoxicity toward 721.221 cells by both HkRP3-depleted NKL cells (Fig. 2B, *left* and *center panels*) and primary human NK clones (Fig. 2C, *left* and *left center panels*). We also examined cytotoxicity mediated by specific NK-activating receptors (NKG2D or CD16) using P815 target cells in a reverse Ab-dependent cellular cytotoxicity assay. Suppression of HkRP3 consistently decreased redirected cytotoxicity through CD16 (Fig. 2C, *right center panel*) and NKG2D (Fig. 2B, *right panel*, Fig. 2C, *right panel*). Taken together, these data identify HkRP3 as an essential regulator of NK cell–mediated cytotoxicity.

HkRP3 does not affect NK cell/target cell conjugation

An early event during NK cell cytotoxicity is the binding of NK cells to target cells via integrin-mediated adhesion (3). We had previously shown that depletion of DOCK8 in NK cells resulted in a dramatic decrease in NK cell adhesion to target cells (8). To examine whether HkRP3 is involved in conjugate formation, we compared the adhesion of control-transfected and HkRP3-suppressed YTS cells. YTS cells and 721.221 target cells prelabeled with different fluorescent dyes were incubated together at

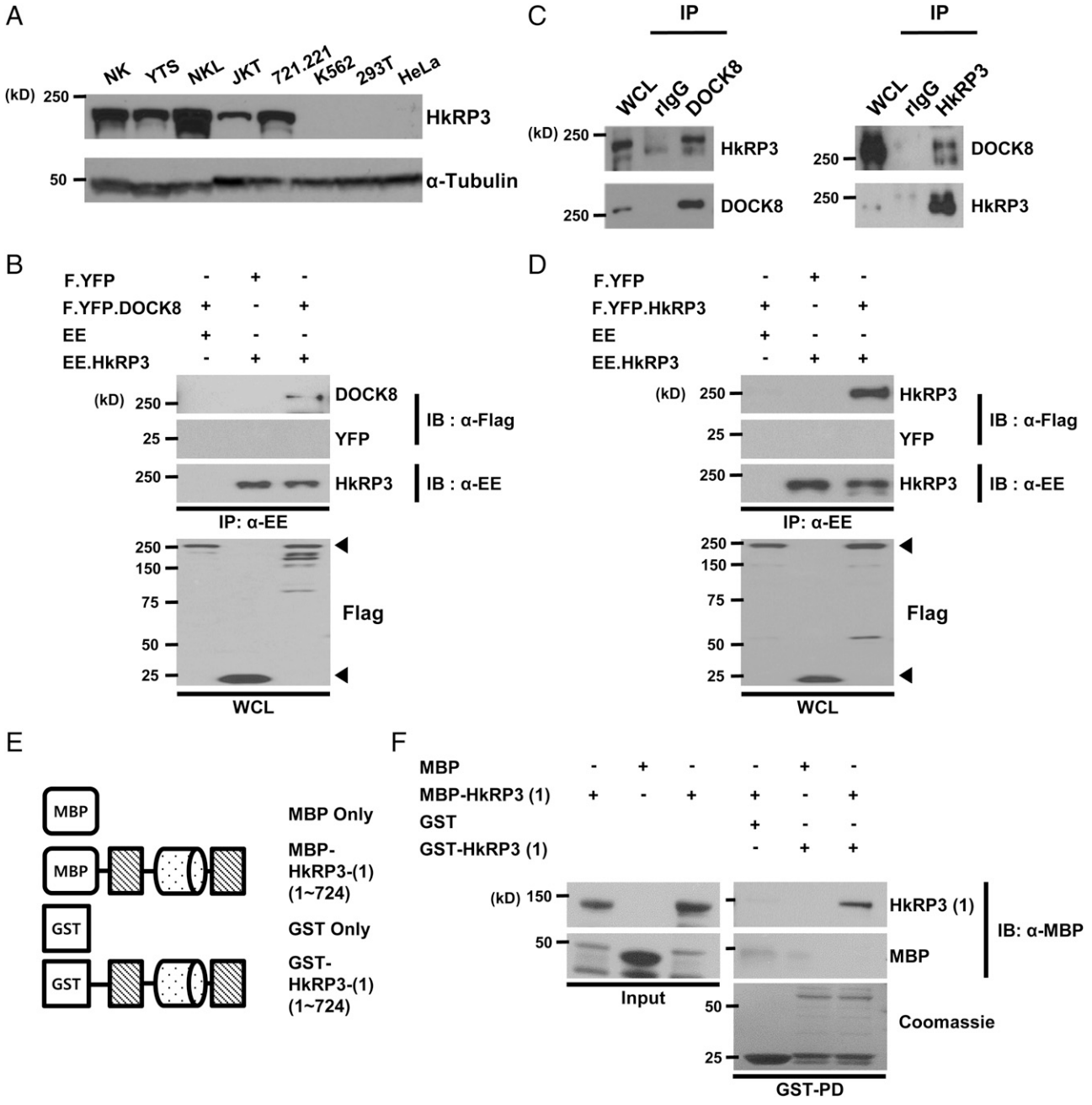

FIGURE 1. HkRP3 is expressed in NK cells, interacts with DOCK8, and forms an oligomer. (**A**) Immunoblot for HkRP3 in whole-cell lysates from a primary human NK clone, human NK cell lines (NKL and YTS), and other cell lines (*top panel*). Immunoblot for α-tubulin is shown as a loading control (*bottom panel*). JKT, Jurkat T cells; 293T, 293T human embryonic kidney cells. (**B**) HEK293T cells were transfected with the indicated plasmids. Two days posttransfection, cell lysate was immunoprecipitated with anti-EE and examined for DOCK8 (FLAG). Arrowheads denote bands of FLAG-tagged proteins from whole-cell lysates (WCL). (**C**) Immunoblot analysis of whole-cell lysates with anti-DOCK8 or anti-HkRP3 immunoprecipitates (IP) derived from YTS cells. IP with rabbit IgG (rIgG) was used as a negative control. (**D**) HEK293T cells were transfected with the indicated plasmids. Two days post-transfection, cell lysate was immunoprecipitated with anti-EE and examined for HkRP3 (FLAG). Arrowheads denote bands of FLAG-tagged proteins from whole-cell lysates (WCL). (**E**) Schematic representation of HkRP3 fragments used for GST pull-down assays in (**F**). Cylinder shape represents coiled-coil region. (F) MBP or MBP-HkRP3(1) (aa 1–724) were pulled down by GST or GST-HkRP3(1) (aa 1–724) as denoted above the lanes and examined for MBP or HkRP3 by immunoblot (*top* and *middle panels*). Coomassie blue staining shows GST fusion proteins used in the pull-down assay (*bottom panel*). Data shown are representative of three independent experiments.

37˚C and the percentage of target-bound YTS cells was measured using flow cytometry. In contrast to DOCK8 depletion, which abrogated NK cell adhesion, HkRP3-suppressed YTS cells showed as efficient conjugate formation as did control cells, suggesting that HkRP3 does not mediate conjugate formation of NK cells to target cells (Fig. 3A). In addition to increased affinity maturation via conformational change, integrins are also observed to accumulate at the center of the NK/target interface contributing to the formation of the CS (3). Therefore, we examined whether LFA-1 (CD11a/CD18) accumulation at the CS is normal in HkRP3-suppressed YTS cells. After 25 min of incubation of YTS cells with prelabeled 721.221 cells, cells were fixed and stained for LFA-1 (Fig. 3B). Consistent with results from the conjugate formation assay, HkRP3-depleted YTS cells presented normal polarization of LFA-1 to the CS, similar to control YTS cells (Fig. 3B, 3C). However, as expected (8), most of the DOCK8-

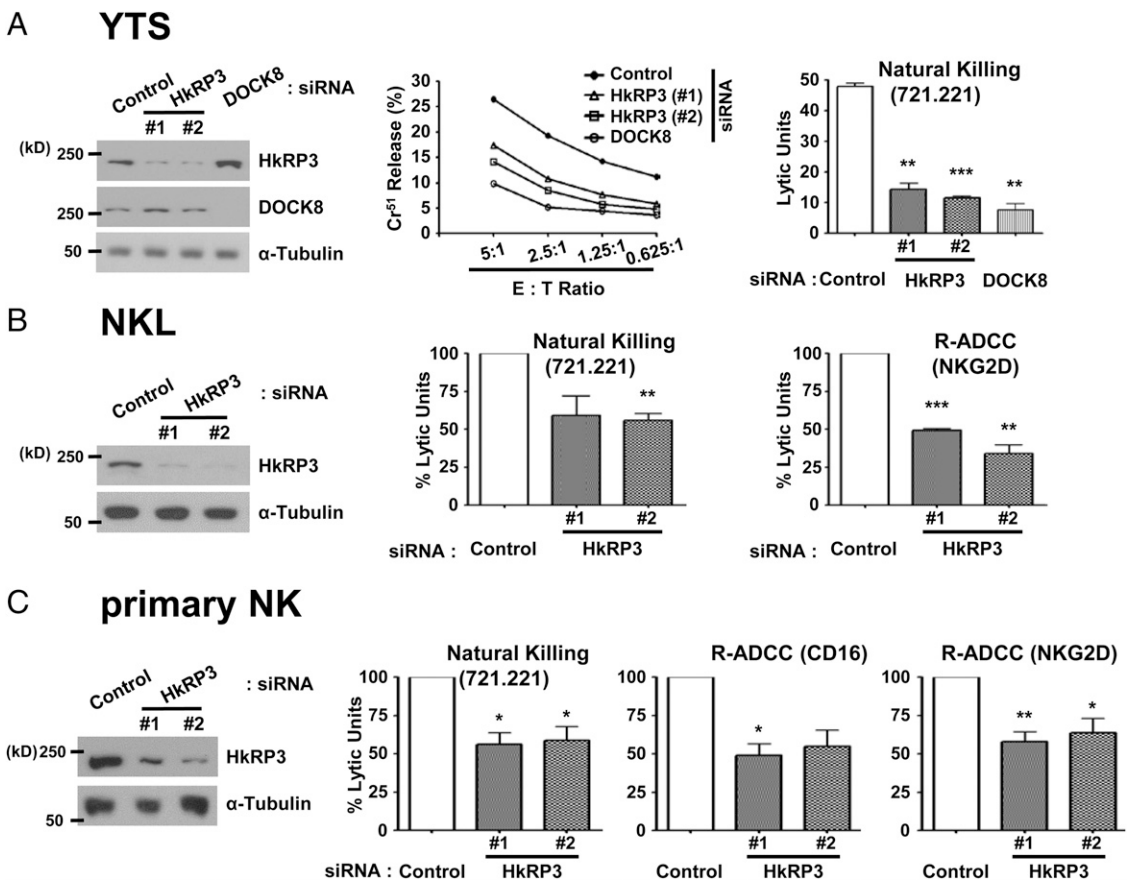

FIGURE 2. HkRP3 mediates NK cell cytotoxicity. (**A**–**C**) The indicated NK cell types were nucleofected with control, HkRP3, or DOCK8 siRNAs. Seventy-two hours after nucleofection, cell lysates were prepared and immunoblotted with the indicated Abs (*left panels*). (A) Nucleofected YTS cells were incubated with ^{51}Cr-labeled 721.221 cells and the percentage specific release was measured over the indicated E:T ratios (*center panel*). Cytotoxic activity of control, HkRP3-, or DOCK8-depleted YTS cells was assessed and expressed as LUs (*right panel*). Data shown are representative (*left* and *center panels*) or average (*right panel*) of three independent experiments. (B) LU values of NKL cells transfected with the indicated siRNA oligonucleotides against 721.221 target cells (*center panel*) or P815 target cells coated with anti-NKG2D (*right panel*) were calculated and presented as a percentage of LU values of the control group. Data shown are representative (*left panel*) or an average of three independent experiments. (C) LU values of primary human NK clones transfected with the indicated siRNA oligonucleotides against 721.221 (*left center panel*) or P815 target cells coated with anti-CD16 (*right center panel*) or anti-NKG2D (*right panel*) were calculated and presented as a percentage of LU values of the control group. Data shown are representative (*left panel*) or an average of three (721.221 and CD16) and four (NKG2D) independent experiments. Error bars indicate SEM. $*p < 0.05$, $** p < 0.01$, $***p < 0.005$ compared with control group.

depleted YTS cells failed to polarize LFA-1 to the CS. Taken together, these data indicate that HkRP3 is an important regulator of NK cell–mediated cytotoxicity, but it is not involved in the initial step of conjugate formation.

HkRP3 regulates convergence of lytic granules to the MTOC

Because loss of DOCK8 impacts MTOC polarization during NK cell killing, we next examined whether HkRP3 might regulate the polarization of lytic granules toward the CS. During NK cytotoxicity, two different steps of lytic granule polarization occur: 1) lytic granules rapidly accumulate around the MTOC as NK cells interact with target cells, and 2) the MTOC along with the converged lytic granules polarize toward the CS (3, 6). In most cases, a 25-min incubation of control-transfected YTS cells with 721.221 targets resulted in lytic granules (visualized by perforin stain, red) clustering around the MTOC (visualized by γ-tubulin stain, green) and polarization of the MTOC just behind the NK/target interface (Fig. 4A, *left panel*). In the case of DOCK8-depleted YTS cells, lytic granules converged around the MTOC, but the MTOC failed to polarize toward the CS in many conjugates, similar to what was observed previously (Fig. 4A, *right panel*) (7, 8). Surprisingly, in the case of HkRP3-suppressed YTS cells, not only did lytic granules fail to cluster around the MTOC, but the MTOC itself was also found to be distant from the CS (Fig. 4A, *middle panel*). To quantify the defective lytic granule clustering around the MTOC in HkRP3-depleted YTS cells, we measured the mean distance of lytic granules to the MTOC (see *Materials and Methods*) (Fig. 4B, *top panel*). Because we could not distinguish which individual conjugated YTS cells are successfully siRNA depleted for our gene of interest due to limitations in Ab options, we placed the conjugated YTS cells into groups depending on the measured distances and calculated the percentage of incidences (Fig. 4B, *bottom panel*). The mean lytic granule to MTOC distance of most conjugated control YTS cells fell within the range of 1–2 μm, and about a third of the conjugated cells displayed distances of <1 μm. In the case of both HkRP3- and DOCK8-depleted YTS cells, most of the mean distances of lytic granules from the MTOC also fell within the range of 1–2 μm, similar to the control group. However, many of the HkRP3-depleted YTS cells presented mean granule to MTOC distances of >2 μm (Fig. 4B, *bottom panel*). Unexpectedly, many DOCK8-depleted YTS cells displayed very tight clustering of lytic granules toward the MTOC when conjugated, having the average distance of granule to MTOC of <0.5 μm (Fig. 4A, 4B, *bottom panel*). We

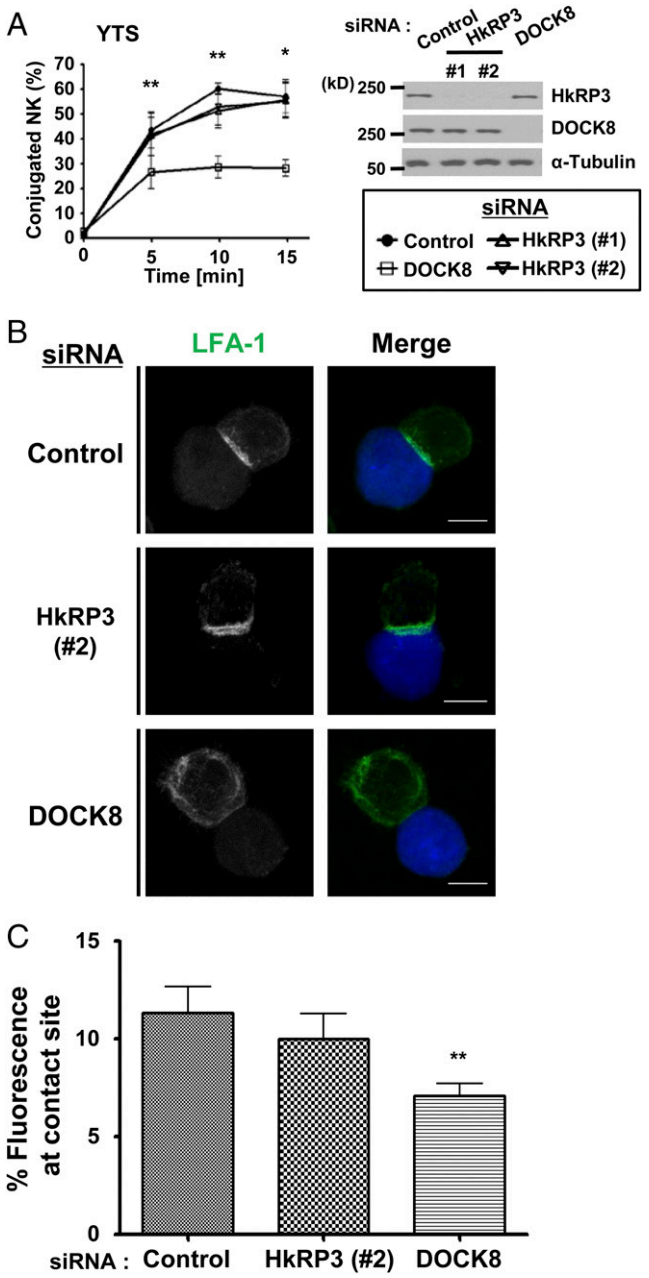

FIGURE 3. HkRP3 does not modulate NK conjugate formation. (**A**) YTS cells were nucleofected with the indicated siRNAs. Seventy-two hours after nucleofection, YTS cells were stained with CellTracker Violet and then incubated with CFSE-labeled 721.221 cells for the indicated times at 37˚C. The percentage of conjugated YTS cells was assessed using two-color flow cytometry and calculated based on simultaneous emission of both violet and green fluorescence. Presented data are the average of four independent experiments performed in duplicate or triplicate. Error bars indicate SEM. $*p < 0.05$, $**p < 0.01$ compared with control group. (**B** and **C**) YTS cells were transfected with the indicated siRNA oligonucleotides. At 72 h, these cells were conjugated with CMAC-stained 721.221 target cells (blue), incubated for a total of 25 min at 37˚C, and fixed for immunofluorescence staining. (B) Representative images from three independent experiments (LFA-1, green). Scale bars, 10 μm. (C) Scoring of LFA-1 polarization to the YTS/721.221 interface (see *Materials and Methods*). Data shown are collected from three independent experiments. Error bars indicate SEM. $**p < 0.01$ compared with control group.

also measured the distance between the MTOC and the center of the CS to represent the degree of polarization of the MTOC to the CS (Fig. 4C, *top panel*). Almost half of the conjugated control YTS cells displayed MTOC distances close to the CS (0–5 μm) (Fig. 4C, *bottom panel*). In the case of both HkRP3- and DOCK8-depleted YTS cells, however, the MTOCs of many conjugated YTS cells were found to be distant from the CS (>10 μm). These findings suggest that HkRP3 mediates lytic granule clustering to the MTOC as well as MTOC polarization to the CS. It further shows that DOCK8 depletion does not impact lytic granule clustering, and it may in fact negatively regulate this step in the cytotoxic process.

Previously, it was shown that the clustering of lytic granules to the MTOC could be triggered by stimulation of NK activation receptors alone (6, 23). In the case of YTS cells, whereas stimulation of nonactivating receptor CD45 does not cause convergence of lytic granules to the MTOC, stimulation through CD28 induces lytic granule clustering. To confirm whether HkRP3 regulates lytic granule clustering toward the MTOC, we stimulated YTS cells using anti-CD45– or anti-CD28–coated glass coverslips after depletion of HkRP3 or DOCK8 by siRNA. Following 25 min of incubation on coverslips coated with anti-CD28 Abs, lytic granules from both control- and DOCK8-depleted YTS cells accumulated around the MTOC (Fig. 5A, 5B). Interestingly, lytic granules of many DOCK8-depleted YTS cells were again more tightly clustered to the MTOC (Fig. 5B, *bottom panel*). However, almost half of the HkRP3-depleted YTS cells had a more dispersed distribution of lytic granules (Fig. 5A, 5B). As expected, lytic granules did not cluster when the different groups of YTS cells were placed on anti-CD45 Ab–coated coverslips (Fig. 5C). These data suggest that HkRP3 mediates the clustering of lytic granules to the MTOC in stimulated NK cells.

HkRP3 mediates efficient transport of lytic granules to the MTOC

Clustering of lytic granules to the MTOC is dependent on minus-end-directed movement of dynein motors along the MT network (6). Our findings in the previous section clearly suggest an important role of HkRP3 in convergence of lytic granules to the MTOC in stimulated YTS cells (Figs. 4, 5). However, it does not provide detailed information on how MTOC-directed movement of lytic granules is affected when HkRP3 is depleted in NK cells. Does HkRP3 depletion in NK cells completely impair lytic granule transport to the MTOC, or does it affect the kinetics of the transport? To understand the observed phenotype of HkRP3-suppressed YTS cells in more detail, we assessed both accumulation of lytic granules to the MTOC and polarization of the MTOC toward the CS in control or HkRP3-depleted YTS cells conjugated with 721.221 target cells for various lengths of time (Fig. 6). For a more clear presentation of our data, we present averaged values of both the mean distance of lytic granules from the MTOC and the distance of the MTOC to the CS. In the case of control YTS cells, lytic granules were rapidly converged to the MTOC within 10 min of incubation with target cells (Fig. 6A, 6B). This corresponds to the previous finding that lytic granule clustering to the MTOC is an early and rapid event during NK cell activation (6). Alternatively, although the average distance of lytic granules from the MTOC gradually decreased throughout the time course, HkRP3-depleted YTS cells required 30 min to accumulate lytic granules to the MTOC (Fig. 6A, 6B). Additionally, polarization of the MTOC to the CS was achieved later than lytic granule clustering in the case of control YTS cells, consistent with prior observations (Fig. 6A, 6C) (6). The mean distance between MTOC and the CS did not change significantly during the first 10 min of incubation. In later time points, however, most of the conjugated YTS cells displayed clear polarization of the MTOC toward the CS. Interestingly, in the case of HkRP3-depleted YTS

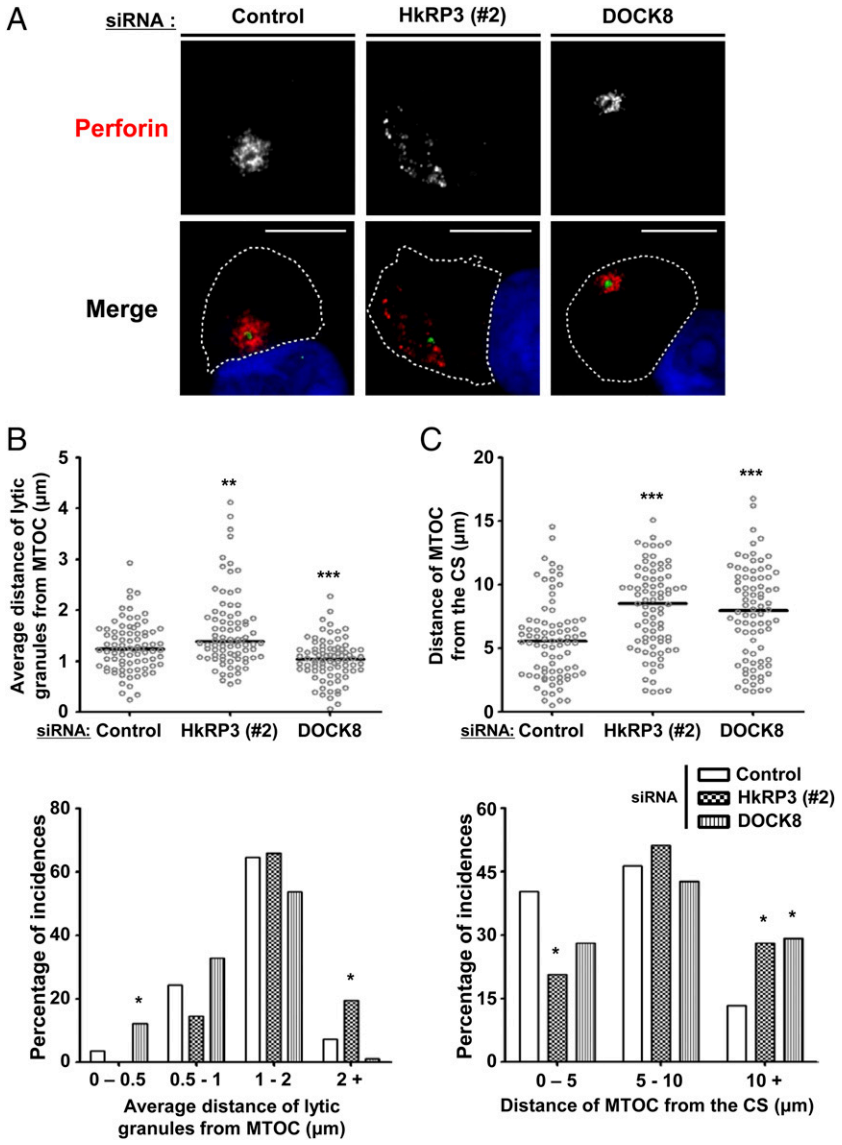

FIGURE 4. HkRP3 regulates lytic granule clustering to the MTOC as well as MTOC polarization to the CS. (**A**–**C**) YTS cells were transfected with the indicated siRNA oligonucleotides. At 72 h, these cells were conjugated with CMAC-stained 721.221 target cells (blue), incubated for a total of 25 min at 37°C, and fixed for immunofluorescence staining. (A) Representative images from five independent experiments (perforin, red, γ-tubulin, green). Scale bars, 10 μm. (B) Average distances of lytic granules from the MTOC were measured from 82 conjugated YTS cells per each experimental group (15–20 conjugated YTS cells per experiment; five independent experiments; see *Materials and Methods*). *Top panel*: Scatter plot of mean distances of lytic granules from the MTOC. Bar indicates median. *Bottom panel*: Percentage of incidences based on mean distances of lytic granules from the MTOC. (C) Distances of the MTOC from the center of the CS were measured from 82 conjugated YTS cells per each experimental group (15–20 conjugated YTS cells per experiment; five independent experiments; see *Materials and Methods* for details). *Top panel*: Scatter plot of distances of the MTOC from the center of the CS. Bar indicates median. *Bottom panel*: Percentage of incidences based on distances of the MTOC from the center of the CS. $*p < 0.05$, $**p < 0.01$, $***p < 0.005$ compared with control group.

cells, the average distance of the MTOC from the CS did not change throughout the time points examined (Fig. 6C). Because we could not completely deplete HkRP3 in YTS cells using siRNA transfection, the delayed transport of lytic granules to the MTOC might be due to the remaining activity of HkRP3. However, considering efficient suppression of HkRP3 (Figs. 2, 3A), it is more likely that HkRP3 mediates processive transport of lytic granules toward the MTOC in activated NK cells. Taken together, these data suggest that HkRP3 regulates efficient transport of lytic granules toward the MTOC.

HkRP3 directly interacts with microtubules through its C-terminal region

We next wanted to determine the localization of HkRP3 in NK cells interacting with target cells. We first confirmed the specificity of our purified rabbit polyclonal Ab toward HkRP3 using YTS cells treated with siRNA control or siHkRP3 (Supplemental Fig. 1). We next examined where HkRP3 is localized in NK cells. Because we have observed defective clustering of lytic granules along the MT network when HkRP3 is absent (Figs. 4–6), we examined localization of HkRP3 along with MTs as well as perforin to identify lytic granules (Fig. 7A). We found strong staining of HkRP3 at the MTOC, as well as discrete puncta along MT filaments (Fig. 7A, *top row*). Although puncta of HkRP3 did not exactly colocalize with perforin, they were often detected adjacent to the perforin-stained lytic granule (Fig. 7A, *second row*, see *inset*). Considering limitations in the lateral resolution of standard confocal microscopy used in this study (250 nm), further examination of endogenous localization of HkRP3 using super-resolution microscopy will be informative.

The finding that HkRP3 localized to the MTOC as well as along MTs was interesting, because every Girdin family protein contains a putative MT binding domain at its N terminus (14). Although a similar localization pattern of Girdin has been reported (24), it has not yet been tested whether this homologous region actually binds to MTs. Furthermore, current knowledge suggests potential roles of Girdin family proteins in many different aspects of cell biology, but not in MT regulation or cargo transport along MTs. To determine whether HkRP3 directly interacts with MTs and to map the binding region, we performed a pelleting assay with in vitro polymerized MTs. Unexpectedly, within tested concentrations of MTs, the N-terminal region of HkRP3 did not co-pellet with MTs (Supplemental Fig. 2A). Because HkRP3 contains a unique region at the C terminus, we next tested the possibility that the unique region is responsible for the direct interaction of HkRP3 with MTs. Although the C-terminal region of HkRP3

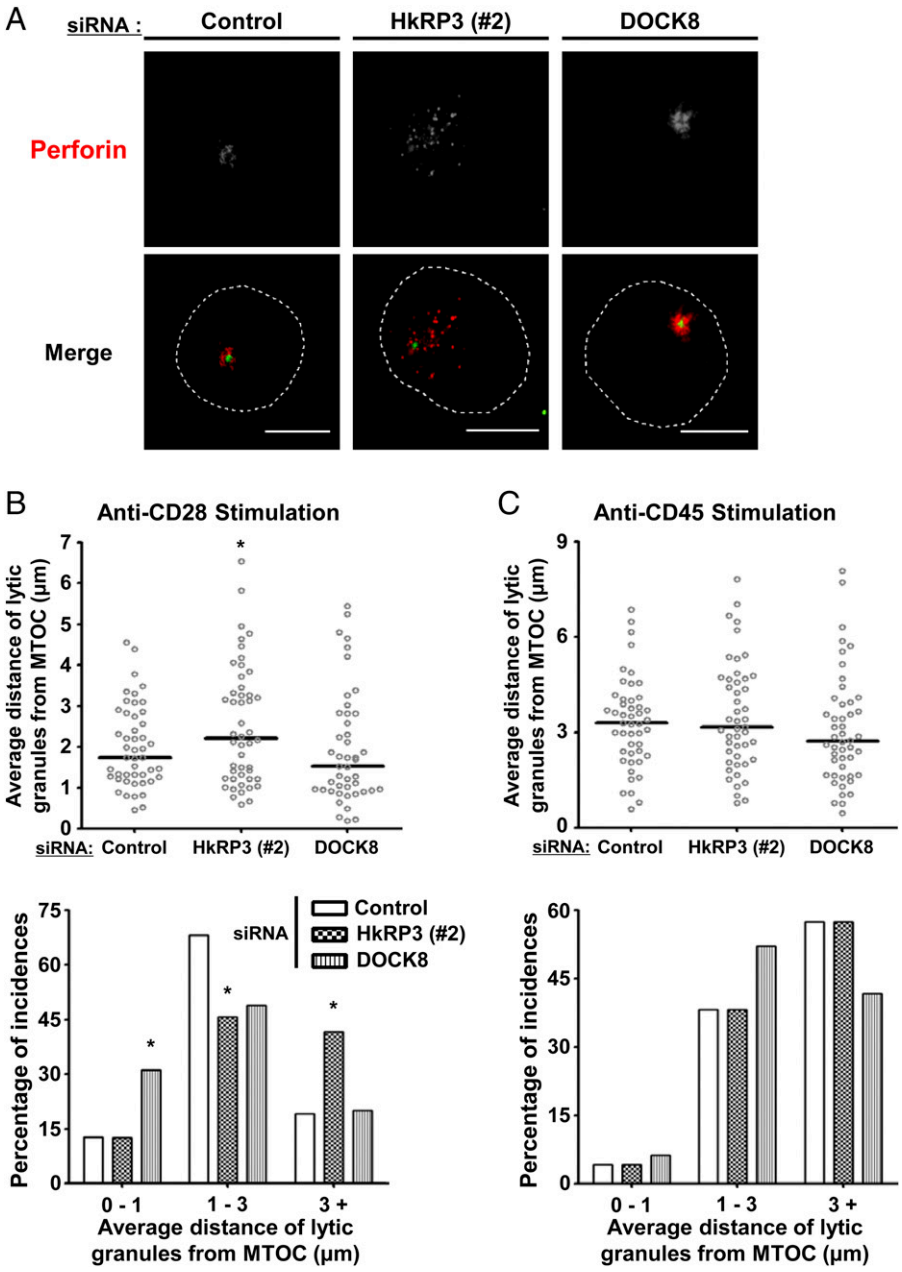

FIGURE 5. HkRP3 mediates lytic granule clustering to the MTOC after stimulation with anti-CD28. (**A**–**C**) At 72 h after siRNA transfection into YTS cells as indicated, cells were placed on anti-CD28–coated (A and B) or anti-CD45–coated (C) coverslips, incubated for 25 min at 37°C, and fixed for immunofluorescence staining. (A) Representative images from three independent experiments with anti-CD28 stimulation (perforin, red; γ-tubulin, green). Scale bars, 10 μm. (B and C) Average distances of lytic granules from the MTOC were measured from 45 to 48 YTS cells per each experimental group (15–20 conjugated YTS cells per experiment; three independent experiments; see *Materials and Methods*). *Top panels*: Scatter plot of mean distances of lytic granules from the MTOC. Bar indicates median. *Bottom panels*: Percentage of incidences based on mean distances of lytic granules from the MTOC. $*p < 0.05$ compared with control group.

fused with GST was not pelleted by itself (Fig. 7B, 7C), it was co-pelleted when incubated with MTs, consistent with the idea that HkRP3 can interact with MTs and its punctate localization with MTs in cells. This was not due to nonspecific interaction of GST with microtubules, because GST was not co-pelleted with MTs (Fig. 7C). Because HkRP3 directly interacts with MTs, it is possible that the impaired clustering of lytic granules in HkRP3-depleted YTS cells might be due to disruption of the MT network. However, when we examined the gross MT network in HkRP3-depleted YTS cells, we did not notice any conspicuous difference in HkRP3-suppressed YTS cells compared with control cells (Supplemental Fig. 1B). These data demonstrate that HkRP3 directly interacts with MTs through its C-terminal unique region of HkRP3.

HkRP3 interacts with the dynein/dynactin MT motor complex

Dynein is an ~1.2-MDa multisubunit motor responsible for most of the minus end–directed transport of diverse cargoes along the MT network in eukaryotic cells (25). Dynein requires the dynactin complex for its cellular functions and exists as a dynein/dynactin complex (called dynein complex hereafter). Dynactin is considered an essential regulator of dynein by mediating the cellular localization of dynein, selection of its cargoes, and motor processivity. Significantly, the dynein complex is responsible for lytic granule clustering to the MTOC in NK and $CD8^+$ T cells (6, 26). Therefore, we speculated that HkRP3 might play a role in regulating motor activity of the dynein complex in addition to its interaction with MTs. Importantly, we could confirm the endogenous interaction of HkRP3 with DIC, a component of the dynein motor, as well as with $p150^{Glued}$, which is a subunit of dynactin (Fig. 7D). The interactions of HkRP3 with these subunits might be due to, or dependent on, the interaction of HkRP3 with MTs, because the dynein complex also directly binds MTs. However, this was found not to be the case, as endogenous HkRP3 still co-precipitated with $p150^{Glued}$ in YTS cells even after nocodazole-induced destabilization of the MT network (Fig. 7D, Supplemental Fig. 2B). As indicated above, HkRP3 contains an N-terminal region, two coiled-coil domains in the middle, and a unique C-terminal

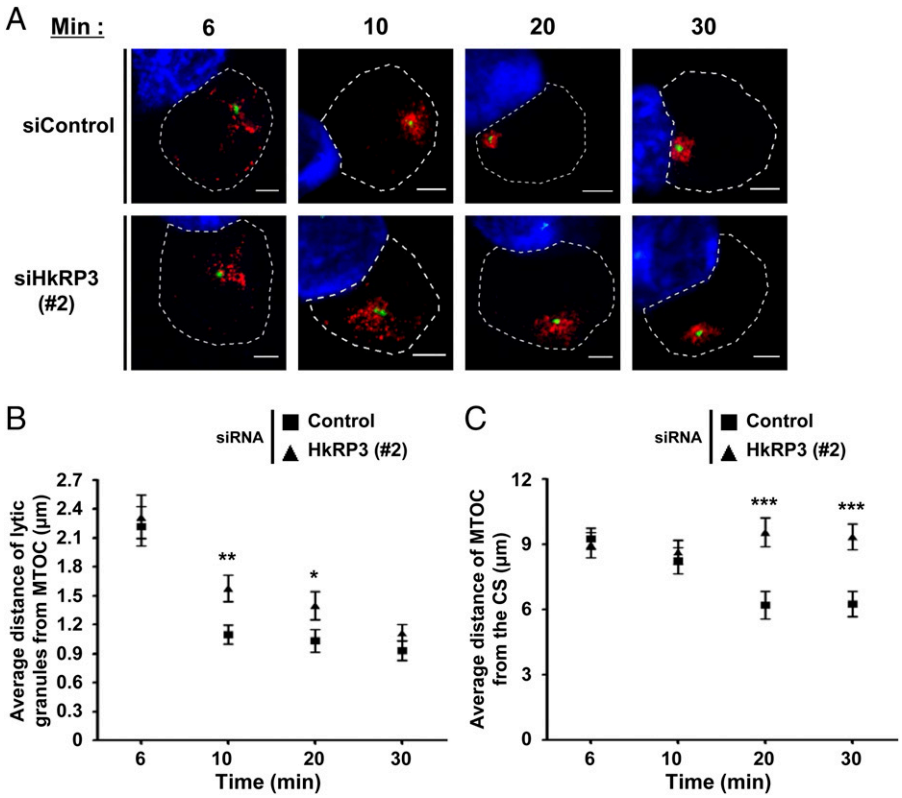

FIGURE 6. HkRP3 regulates efficient transport of lytic granules to the MTOC. (**A**–**C**) Seventy-two hours after siRNA nucleofection, YTS cells were conjugated with CMAC-stained 721.221 target cells (blue), incubated for the indicated times at 37˚C, and fixed for immunofluorescence staining. (A) Representative images from three independent experiments (perforin, red; γ-tubulin, green). Scale bars, 5 μm. (B) Average distances of lytic granules from the MTOC were measured for 30–35 conjugated YTS cells per experimental group (10–12 conjugates per experiment; three independent experiments) and averaged. (C) Distances of the MTOC from the center of the CS were measured for 30–35 conjugated YTS cells per time point (10–12 conjugates per experiment; three independent experiments) and averaged. Error bars indicate SEM. *$p < 0.05$, ** $p < 0.01$, ***$p < 0.005$ compared with control group.

region (14, 15). To delineate the interacting region of HkRP3 with dynein motor complex subunits, we designed four nonoverlapping fragments of HkRP3 fused with GST at the N terminus (Fig. 7B). Then, using a GST pull-down assay, we mapped the interacting region of HkRP3 for each subunit of the dynein complex (Fig. 7E). DIC was mainly pulled down with the C terminus of HkRP3. Alternatively, $p150^{Glued}$ was equally pulled down with both the C terminus and the second half of the coiled-coil region. Next, we compared endogenous localization patterns of HkRP3 with those of DIC as well as $p150^{Glued}$. Both DIC and $p150^{Glued}$ appeared as puncta aligning with the MT network similar to HkRP3 (Fig. 7A, *third* and *fourth rows*), but their staining patterns did not exactly overlap. Taken together, these data indicate that HkRP3 interacts with the dynein motor complex.

Inefficient transport of lytic granules toward the MTOC in the absence of HkRP3 in NK cells (Fig. 6) suggests that regulation of dynein motor activity might be impaired in HkRP3-depleted NK cells. As dynactin is known to be important for dynein processivity (25, 27), one possibility is that HkRP3 might be important for the stable interaction between dynein and dynactin. Based on the assumption that HkRP3 might mediate most of the transport activity of the dynein complex in NK cells, we tested whether the interaction of the dynein motor with dynactin is affected in HkRP3-depleted NKLs following receptor stimulation. However, as shown in Supplemental Fig. 3A, DIC immunoprecipitated similar levels of $p150^{Glued}$ throughout the time course in both control and HkRP3-depleted NKL cells.

HkRP3 is found in the lytic granule fraction

Previously, Mentlik et al. (6) reported that the dynein complex is constitutively localized at lytic granules of NK cells. Because HkRP3 not only interacts with dynein complex but also seems to regulate dynein complex–mediated lytic granule clustering along MTs, we questioned whether HkRP3 might also be localized at the lytic granules of NK cells. To determine the presence of HkRP3 in lytic granules, the lysosomal fraction was purified from YTS cells and evaluated by immunoblot (Fig. 7F). As shown, granzyme B, a major cytotoxic component of lytic granules, was detected only in the crude lysosomal fraction, whereas β-actin was abundant only in the nonlysosomal fraction. Interestingly, HkRP3 as well as the dynein complex subunits were also detected in the crude lysosomal fraction. Therefore, a fraction of HkRP3 copurifies with lytic granules.

In nonimmune cells, it was previously demonstrated that Rab-interacting lysosomal protein (RILP) recruits dynein complex to the late endosome/lysosome in association with Rab7 and oxysterol-binding protein-related protein 1L (28, 29). Interestingly, Rab7 and RILP localized at lytic granules in T cells and YTS cells, and $CD8^+$ T cells overexpressing RILP displayed clustered lytic granules (26, 30, 31). It is possible that cytotoxic lymphocytes use HkRP3 as an additional regulator to recruit or dock the dynein complex to lytic granules. However, this was not the case, because localization of the dynein complex subunits did not seem to be affected when HkRP3 was depleted (Supplemental Fig. 3B), nor did it affect the intracellular levels of perforin or granzyme B (Supplemental Fig. 3C). Taken together, our data suggest that some proportion of HkRP3 constitutively associates with lytic granules to facilitate their efficient transport along MTs (Fig. 8).

Discussion

Previously, it was demonstrated in endothelial cells that HkRP3 mediates ER stress response via its interaction with GRP78, so HkRP3 was named Gipie (GRP78-interacting protein induced by ER stress). However, considering its preferential expression in immune cells as well as its roles in NK cells that are similar to the general functions of Hook proteins, we prefer to keep its name as Hook-related protein 3 (HkRP3) as originally suggested by Simpson et al. (24). In this study, we show that HkRP3, a novel DOCK8-interacting protein, is essential for NK cell–mediated cytotoxicity through its effects on lytic granule transport and

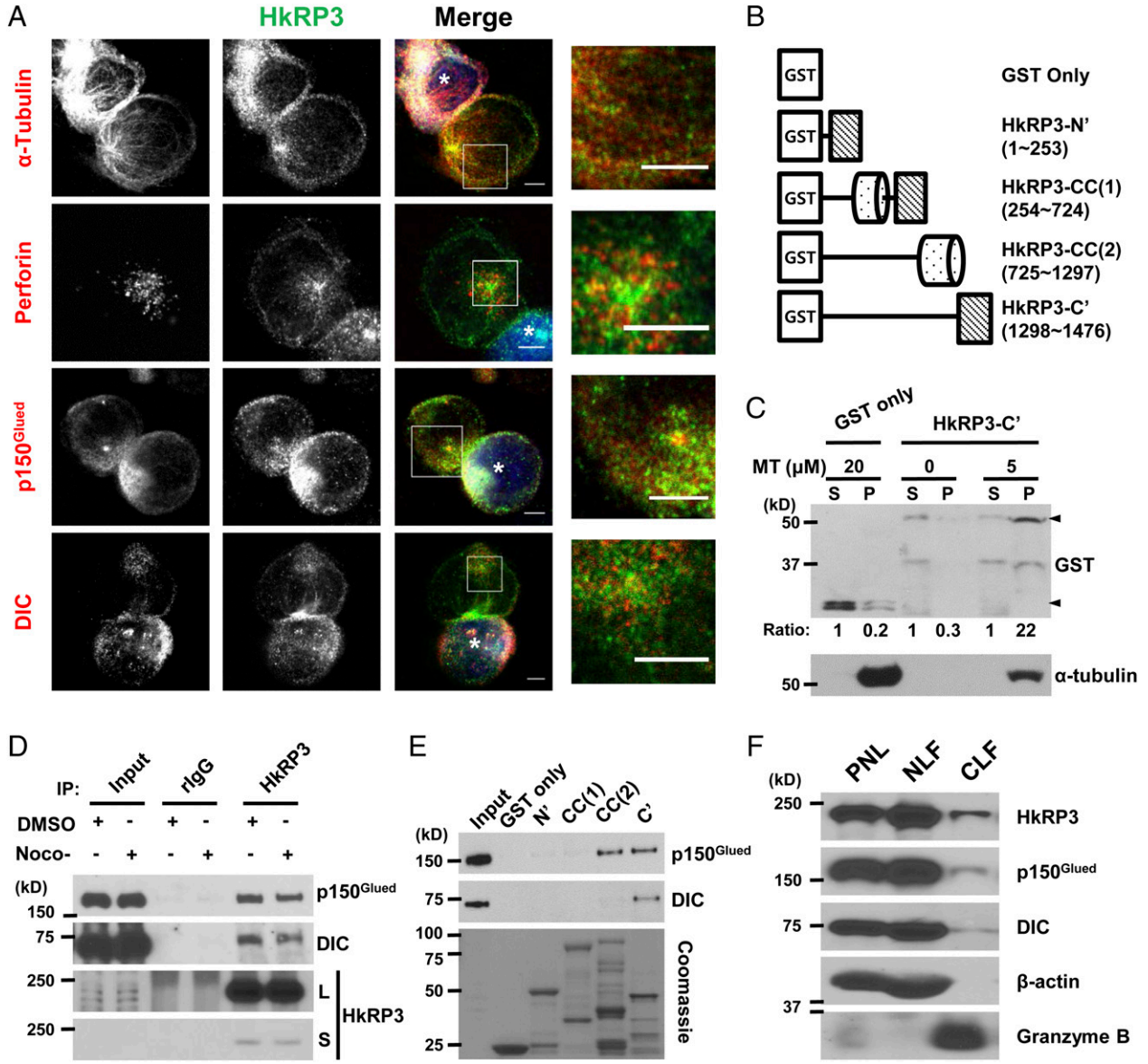

FIGURE 7. HkRP3 exists in lytic granules, binds microtubules, and interacts with the dynein motor complex. (**A**) YTS cells were conjugated with CMAC-stained 721.221 target cells (blue, marked with white asterisk), incubated for a total of 25 min at 37˚C, and fixed for immunofluorescence staining with the indicated Abs. Images are representative of three independent experiments. Scale bars, 5 μm. (**B**) Schematic representation of HkRP3 fragments used for MT co-pelleting assay (**C**) and GST pull-down assays (**E**). Cylinder shape represents coiled-coil region. (C) Microtubule co-pelleting assay; 0.5 μM of either GST or GST-HkRP3-C′ was incubated with MTs of indicated concentrations. After centrifugation, supernatants (S) and pellets (P) were collected and examined for α-tubulin and GST by immunoblot. Arrowheads denote GST-fusion proteins. The numbers beneath the GST blot provide a densitometric ratio of each signal from the supernatant fraction within the same sample group. Data shown are representative of three independent experiments. (**D**) YTS cells were treated with 10 μM nocodazole or the same volume of DMSO for 1 h at 37˚C and washed. Some cells were fixed for immunofluorescence staining for α-tubulin to confirm disruption of the microtubule network (Supplemental Fig. 2B). The remaining cells were lysed and immunoprecipitated using anti-HkRP3. Immunoprecipitation (IP) with rabbit IgG (rIgG) was used as a negative control. Whole-cell lysates and immunoprecipitates were examined for HkRP3, p150^{Glued}, and DIC. Data shown are representative of five independent experiments. L, long exposure; S, short exposure. (E) Lysates from YTS cells were pulled down by GST or GST-HkRP3 fragments and examined for p150^{Glued} and DIC by immunoblot. Coomassie blue staining shows GST fusion proteins used in the pull-down assay (*bottom panel*). Data shown are representative of three independent experiments. (**F**) Postnuclear lysate (PNL), nonlysosomal fraction (NLF), and crude lysosomal fraction (CLF) were prepared from YTS cells and examined for HkRP3, p150^{Glued}, DIC, β-actin, and granzyme B by immunoblot. Data shown are representative of three independent experiments.

MTOC polarization. Interestingly, HkRP3 appeared as puncta coating the MT network and was found to accumulate at the MTOC. Using a biochemical approach, we show that the C terminus of HkRP3, which is not shared among Girdin family proteins, directly interacts with MTs, whereas the N terminus of HkRP3 is involved in oligomerization (minimally existing as a homodimer), similar to Girdin and Hook proteins (22, 32). Finally, we show that HkRP3 interacts with the dynein motor complex and it remains likely that this interaction is required for lytic granule clustering. Taken together, these findings reveal a novel regulatory molecule that is critical for NK cell cytotoxicity (Fig. 8).

Our findings support the idea that clustering of lytic granules to the MTOC is dynein mediated and is an early and rapid event in NK cell cytotoxicity (6). Under two different experimental conditions, suppression of HkRP3 in YTS cells impaired rapid clustering of lytic granules, which is also observed when dynein motor function

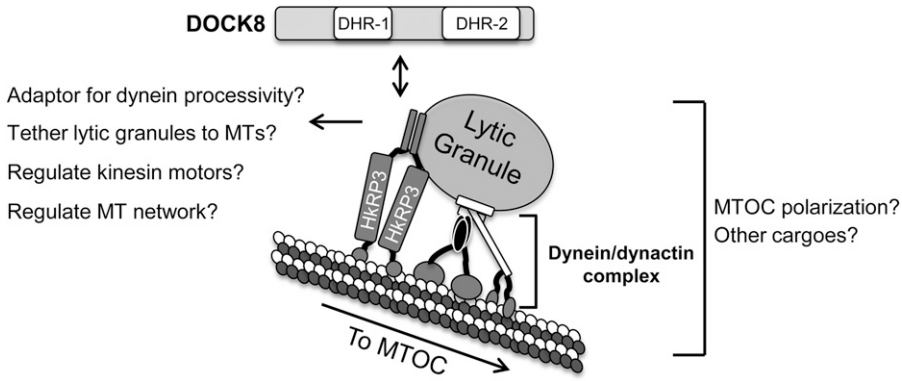

FIGURE 8. Hypothetical model for how HkRP3 mediates lytic granule transport to the MTOC. See text for details.

is inhibited in NK cells. Additionally, the localization pattern of HkRP3 along MTs, the presence of HkRP3 in the lysosomal fraction, and interaction of HkRP3 with dynein motor complex all strongly suggest a close relationship of HkRP3 with the dynein motor complex in regulating the transport of lytic granules in NK cells. Our data indicate that the loss of HkRP3 did not affect the interaction of dynein with dynactin. Moreover, we observed no effect on the accumulation of either component in the lytic granule fraction in the absence of HkRP3. However, it remains possible that while the dynein motor complex is tethered to its cargo, the processivity of the motor is not appropriately regulated in the absence of HkRP3. In fact, it was recently shown that the mammalian dynein/dynactin motor requires adaptor proteins to induce processive motility along MTs (33). Interestingly, the addition of Hook3 substantially increased the processivity of the dynein motor complex. Thus, although the dynein complex is constitutively localized at lytic granules in NK cells, it remains possible that the interaction of HkRP3 with the dynein motor complex would enhance its processive motor function leading to rapid lytic granule clustering to the MTOC. Importantly, note that Hook proteins have been suggested to mediate the tethering of different cargoes to the MT network (32, 34). They mediate this by binding to MTs using their highly conserved N termini, and they bind to their cargoes (organelles or proteins) via their more divergent C termini. Similar domain organization of Hook proteins to that of CLIP-170, prototypic cytoplasmic linker protein, also supports potential roles of Hook proteins as another group of cytoplasmic MT linker proteins. Girdin family proteins also present similar domain organization to Hook proteins, although conservation between the two families of proteins is limited to the N terminus, which supposedly mediates interaction with MTs (14). Surprisingly, using a MT pelleting assay we were unable to detect any binding of the N terminus to polymerized MTs. In contrast, we find that HkRP3 directly binds to MTs through its unique region located at the C terminus, whereas the N-terminal "Hook-related" domain appears to promote HkRP3 homo-oligomerization. Therefore, HkRP3 is likely minimally a homodimer that acts as a MT-linker protein tethering lytic granules to the MT network either constitutively or in an activation-dependent manner (Fig. 8).

Understanding how HkRP3 cooperates with DOCK8 to mediate NK cell cytotoxicity will be another interesting topic for future studies. Although we mainly focused on elucidating cellular roles of HkRP3 in NK cell cytotoxicity in this study, observations from DOCK8-depleted YTS cells that we used as our positive control suggest clues as to how DOCK8 might be involved in the functions of HkRP3. We found that DOCK8-depleted YTS cells present very tight clustering of lytic granules when they are stimulated. This unexpected observation suggests the possibility that DOCK8 might play regulatory roles in HkRP3-mediated lytic granule transport to the MTOC (Fig. 8). It will be interesting to examine whether the absence of DOCK8 affects the dynamic interaction of HkRP3 with MTs and the dynein complex, and thereby the kinetics of lytic granule transport to the MTOC.

Our data also suggest a role for HkRP3 in MTOC polarization following NK activation. In fact, although our time course experiments revealed that lytic granule convergence to the MTOC is delayed in the absence of HkRP3, MTOC polarization to the CS did not occur. A recent report has indicated that MTOC polarization to the synapse can occur independent of lytic granule clustering (6), and thus HkRP3 is likely impacting both steps in this tightly regulated process. Interestingly, the dynein motor complex has been shown to regulate MTOC polarization in T cells (35–37). Importantly, note the essential roles of CDC42 in MTOC polarization partly by regulating dynein motors (38–42). Considering that DOCK8 is a guanine nucleotide exchange factor for CDC42, future studies focusing on roles of HkRP3 in MTOC polarization to the CS and its relationship with the dynein complex as well as with DOCK8 will provide a better understanding of the mechanism by which HkRP3 regulates MTOC polarization.

HkRP3 might also regulate the transport of lytic granules by coordinating not only motor activity of dynein but also that of kinesins, which are plus-end MT motors. Kinesin-1 has been suggested to mediate MTOC polarization of NK cells and final transport of lytic granules close to accumulated F-actin at the immune synapse of $CD8^+$ T cells (43, 44). Although roles of kinesin motors in regulating transport of lytic granules along MTs have not been examined in detail, it is logical to hypothesize that rapid movement of lytic granules along the MT network also requires kinesin-mediated anterograde transport. Rapid lytic granule clustering was demonstrated to occur in both cytolytic and noncytolytic activation of NK cells, suggesting that the event might act as another checkpoint of NK cytotoxicity (6). When NK cells return to the resting state following activation, they require anterograde motor activity to disperse the lytic granules. Although we only examined the interaction of HkRP3 with dynein complex in this study, it is worthwhile to test whether HkRP3 also regulates kinesin activities. It is very interesting that Hok1, the fungus homolog of Hook proteins, was recently demonstrated to act as an adaptor for early endosome transport by coordinating activities of both dynein and kinesin-3 (45).

While revising our manuscript, HkRP3 (CCDC88B) was identified as a gene responsible for pathological inflammation via a genome-wide screen of *N*-ethyl-*N*-nitrosourea–mutagenized mice (46). Loss of HkRP3 was found to induce resistance in an experimental cerebral malaria model, which normally leads to severe inflammatory responses and lethality. Interestingly, HkRP3 was found to be important for maturation of activated T cells as well as production of inflammatory cytokines. Essential roles of

HkRP3 in NK cell cytotoxicity demonstrated in our study provide another layer of explanation why HkRP3 mutant mice presented protection from experimental cerebral malaria. However, it is not clear at this moment whether potential roles of HkRP3 in regulating dynein complex are also responsible for the observed T cell defects. The molecular mechanism by which HkRP3 mediates T cell maturation and its function requires further studies.

In addition to the points discussed above, several interesting questions need to be answered regarding HkRP3. Some of these include: 1) Does HkRP3 mediate transport of cargoes in immune cells other than lytic granules? 2) Does HkRP3 have any role in regulating the MT network (e.g., posttranslational modification) to mediate cargo transport? Future studies focusing on HkRP3 will provide a better understanding of NK cell cytotoxicity and the mechanistic regulation of MT motors involved in lytic granule clustering and MTOC polarization.

Acknowledgments

We specially thank Debra Evans for technical assistance in the immunofluorescence assay, helpful discussion, and critical reading of the manuscript. The authors are grateful to Joanna Kim for helpful suggestions on quantification of immunofluorescence data. We also thank Cristina Correia for technical advice on purification of recombinant proteins for our in vitro assays. We are also appreciative of the members of the Billadeau laboratory for helpful discussions.

Disclosures

The authors have no financial conflicts of interest.

References

1. Vivier, E., E. Tomasello, M. Baratin, T. Walzer, and S. Ugolini. 2008. Functions of natural killer cells. *Nat. Immunol.* 9: 503–510.
2. Grégoire, C., L. Chasson, C. Luci, E. Tomasello, F. Geissmann, E. Vivier, and T. Walzer. 2007. The trafficking of natural killer cells. *Immunol. Rev.* 220: 169–182.
3. Ham, H., and D. D. Billadeau. 2014. Human immunodeficiency syndromes affecting human natural killer cell cytolytic activity. *Front. Immunol.* 5: 2.
4. Orange, J. S. 2008. Formation and function of the lytic NK-cell immunological synapse. *Nat. Rev. Immunol.* 8: 713–725.
5. Wood, S. M., H. G. Ljunggren, and Y. T. Bryceson. 2011. Insights into NK cell biology from human genetics and disease associations. *Cell. Mol. Life Sci.* 68: 3479–3493.
6. Mentlik, A. N., K. B. Sanborn, E. L. Holzbaur, and J. S. Orange. 2010. Rapid lytic granule convergence to the MTOC in natural killer cells is dependent on dynein but not cytolytic commitment. *Mol. Biol. Cell* 21: 2241–2256.
7. Mizesko, M. C., P. P. Banerjee, L. Monaco-Shawver, E. M. Mace, W. E. Bernal, J. Sawalle-Belohradsky, B. H. Belohradsky, V. Heinz, A. F. Freeman, K. E. Sullivan, et al. 2013. Defective actin accumulation impairs human natural killer cell function in patients with dedicator of cytokinesis 8 deficiency. *J. Allergy Clin. Immunol.* 131: 840–848.
8. Ham, H., S. Guerrier, J. Kim, R. A. Schoon, E. L. Anderson, M. J. Hamann, Z. Lou, and D. D. Billadeau. 2013. Dedicator of cytokinesis 8 interacts with talin and Wiskott-Aldrich syndrome protein to regulate NK cell cytotoxicity. *J. Immunol.* 190: 3661–3669.
9. Engelhardt, K. R., S. McGhee, S. Winkler, A. Sassi, C. Woellner, G. Lopez-Herrera, A. Chen, H. S. Kim, M. G. Lloret, I. Schulze, et al. 2009. Large deletions and point mutations involving the dedicator of cytokinesis 8 (DOCK8) in the autosomal-recessive form of hyper-IgE syndrome. *J. Allergy Clin. Immunol.* 124: 1289–1302, e4.
10. Su, H. C., H. Jing, and Q. Zhang. 2011. DOCK8 deficiency. *Ann. N. Y. Acad. Sci.* 1246: 26–33.
11. Zhang, Q., J. C. Davis, I. T. Lamborn, A. F. Freeman, H. Jing, A. J. Favreau, H. F. Matthews, J. Davis, M. L. Turner, G. Uzel, et al. 2009. Combined immunodeficiency associated with DOCK8 mutations. *N. Engl. J. Med.* 361: 2046–2055.
12. Harada, Y., Y. Tanaka, M. Terasawa, M. Pieczyk, K. Habiro, T. Katakai, K. Hanawa-Suetsugu, M. Kukimoto-Niino, T. Nishizaki, M. Shirouzu, et al. 2012. DOCK8 is a Cdc42 activator critical for interstitial dendritic cell migration during immune responses. *Blood* 119: 4451–4461.
13. Randall, K. L., S. S. Chan, C. S. Ma, I. Fung, Y. Mei, M. Yabas, A. Tan, P. D. Arkwright, W. Al Suwairi, S. O. Lugo Reyes, et al. 2011. DOCK8 deficiency impairs CD8 T cell survival and function in humans and mice. *J. Exp. Med.* 208: 2305–2320.
14. Enomoto, A., J. Ping, and M. Takahashi. 2006. Girdin, a novel actin-binding protein, and its family of proteins possess versatile functions in the Akt and Wnt signaling pathways. *Ann. N. Y. Acad. Sci.* 1086: 169–184.
15. Matsushita, E., N. Asai, A. Enomoto, Y. Kawamoto, T. Kato, S. Mii, K. Maeda, R. Shibata, S. Hattori, M. Hagikura, et al. 2011. Protective role of Gipie, a Girdin family protein, in endoplasmic reticulum stress responses in endothelial cells. *Mol. Biol. Cell* 22: 736–747.
16. Windebank, K. P., R. T. Abraham, G. Powis, R. A. Olsen, T. J. Barna, and P. J. Leibson. 1988. Signal transduction during human natural killer cell activation: inositol phosphate generation and regulation by cyclic AMP. *J. Immunol.* 141: 3951–3957.
17. Banerjee, P. P., R. Pandey, R. Zheng, M. M. Suhoski, L. Monaco-Shawver, and J. S. Orange. 2007. Cdc42-interacting protein-4 functionally links actin and microtubule networks at the cytolytic NK cell immunological synapse. *J. Exp. Med.* 204: 2305–2320.
18. Maasho, K., A. Marusina, N. M. Reynolds, J. E. Coligan, and F. Borrego. 2004. Efficient gene transfer into the human natural killer cell line, NKL, using the Amaxa nucleofection system. *J. Immunol. Methods* 284: 133–140.
19. Gomez, T. S., M. J. Hamann, S. McCarney, D. N. Savoy, C. M. Lubking, M. P. Heldebrant, C. M. Labno, D. J. McKean, M. A. McNiven, J. K. Burkhardt, and D. D. Billadeau. 2005. Dynamin 2 regulates T cell activation by controlling actin polymerization at the immunological synapse. *Nat. Immunol.* 6: 261–270.
20. Piotrowski, J. T., T. S. Gomez, R. A. Schoon, A. K. Mangalam, and D. D. Billadeau. 2013. WASH knockout T cells demonstrate defective receptor trafficking, proliferation, and effector function. *Mol. Cell. Biol.* 33: 958–973.
21. Schenkman, J. B., and D. L. Cinti. 1978. Preparation of microsomes with calcium. *Methods Enzymol.* 52: 83–89.
22. Enomoto, A., H. Murakami, N. Asai, N. Morone, T. Watanabe, K. Kawai, Y. Murakumo, J. Usukura, K. Kaibuchi, and M. Takahashi. 2005. Akt/PKB regulates actin organization and cell motility via Girdin/APE. *Dev. Cell* 9: 389–402.
23. James, A. M., H. T. Hsu, P. Dongre, G. Uzel, E. M. Mace, P. P. Banerjee, and J. S. Orange. 2013. Rapid activation receptor- or IL-2-induced lytic granule convergence in human natural killer cells requires Src, but not downstream signaling. *Blood* 121: 2627–2637.
24. Simpson, F., S. Martin, T. M. Evans, M. Kerr, D. E. James, R. G. Parton, R. D. Teasdale, and C. Wicking. 2005. A novel Hook-related protein family and the characterization of Hook-related protein 1. *Traffic* 6: 442–458.
25. Kardon, J. R., and R. D. Vale. 2009. Regulators of the cytoplasmic dynein motor. *Nat. Rev. Mol. Cell Biol.* 10: 854–865.
26. Daniele, T., Y. Hackmann, A. T. Ritter, M. Wenham, S. Booth, G. Bossi, M. Schintler, M. Auer-Grumbach, and G. M. Griffiths. 2011. A role for Rab7 in the movement of secretory granules in cytotoxic T lymphocytes. *Traffic* 12: 902–911.
27. King, S. J., and T. A. Schroer. 2000. Dynactin increases the processivity of the cytoplasmic dynein motor. *Nat. Cell Biol.* 2: 20–24.
28. Johansson, M., N. Rocha, W. Zwart, I. Jordens, L. Janssen, C. Kuijl, V. M. Olkkonen, and J. Neefjes. 2007. Activation of endosomal dynein motors by stepwise assembly of Rab7-RILP-p150^{Glued}, ORP1L, and the receptor βIII spectrin. *J. Cell Biol.* 176: 459–471.
29. Jordens, I., M. Fernandez-Borja, M. Marsman, S. Dusseljee, L. Janssen, J. Calafat, H. Janssen, R. Wubbolts, and J. Neefjes. 2001. The Rab7 effector protein RILP controls lysosomal transport by inducing the recruitment of dynein-dynactin motors. *Curr. Biol.* 11: 1680–1685.
30. Casey, T. M., J. L. Meade, and E. W. Hewitt. 2007. Organelle proteomics: identification of the exocytic machinery associated with the natural killer cell secretory lysosome. *Mol. Cell. Proteomics* 6: 767–780.
31. Stinchcombe, J. C., E. Majorovits, G. Bossi, S. Fuller, and G. M. Griffiths. 2006. Centrosome polarization delivers secretory granules to the immunological synapse. *Nature* 443: 462–465.
32. Walenta, J. H., A. J. Didier, X. Liu, and H. Krämer. 2001. The Golgi-associated Hook3 protein is a member of a novel family of microtubule-binding proteins. *J. Cell Biol.* 152: 923–934.
33. McKenney, R. J., W. Huynh, M. E. Tanenbaum, G. Bhabha, and R. D. Vale. 2014. Activation of cytoplasmic dynein motility by dynactin-cargo adapter complexes. *Science* 345: 337–341.
34. Maldonado-Báez, L., N. B. Cole, H. Krämer, and J. G. Donaldson. 2013. Microtubule-dependent endosomal sorting of clathrin-independent cargo by Hook1. *J. Cell Biol.* 201: 233–247.
35. Combs, J., S. J. Kim, S. Tan, L. A. Ligon, E. L. Holzbaur, J. Kuhn, and M. Poenie. 2006. Recruitment of dynein to the Jurkat immunological synapse. *Proc. Natl. Acad. Sci. USA* 103: 14883–14888.
36. Liu, X., T. M. Kapoor, J. K. Chen, and M. Huse. 2013. Diacylglycerol promotes centrosome polarization in T cells via reciprocal localization of dynein and myosin II. *Proc. Natl. Acad. Sci. USA* 110: 11976–11981.
37. Yi, J., X. Wu, A. H. Chung, J. K. Chen, T. M. Kapoor, and J. A. Hammer. 2013. Centrosome repositioning in T cells is biphasic and driven by microtubule end-on capture-shrinkage. *J. Cell Biol.* 202: 779–792.
38. Etienne-Manneville, S., and A. Hall. 2001. Integrin-mediated activation of Cdc42 controls cell polarity in migrating astrocytes through PKCζ. *Cell* 106: 489–498.
39. Gomes, E. R., S. Jani, and G. G. Gundersen. 2005. Nuclear movement regulated by Cdc42, MRCK, myosin, and actin flow establishes MTOC polarization in migrating cells. *Cell* 121: 451–463.
40. Palazzo, A. F., H. L. Joseph, Y. J. Chen, D. L. Dujardin, A. S. Alberts, K. K. Pfister, R. B. Vallee, and G. G. Gundersen. 2001. Cdc42, dynein, and dynactin regulate MTOC reorientation independent of Rho-regulated microtubule stabilization. *Curr. Biol.* 11: 1536–1541.

41. Schmoranzer, J., J. P. Fawcett, M. Segura, S. Tan, R. B. Vallee, T. Pawson, and G. G. Gundersen. 2009. Par3 and dynein associate to regulate local microtubule dynamics and centrosome orientation during migration. *Curr. Biol.* 19: 1065–1074.
42. Yuseff, M. I., A. Reversat, D. Lankar, J. Diaz, I. Fanget, P. Pierobon, V. Randrian, N. Larochette, F. Vascotto, C. Desdouets, et al. 2011. Polarized secretion of lysosomes at the B cell synapse couples antigen extraction to processing and presentation. *Immunity* 35: 361–374.
43. Tuli, A., J. Thiery, A. M. James, X. Michelet, M. Sharma, S. Garg, K. B. Sanborn, J. S. Orange, J. Lieberman, and M. B. Brenner. 2013. Arf-like GTPase Arl8b regulates lytic granule polarization and natural killer cell-mediated cytotoxicity. *Mol. Biol. Cell* 24: 3721–3735.
44. Kurowska, M., N. Goudin, N. T. Nehme, M. Court, J. Garin, A. Fischer, G. de Saint Basile, and G. Ménasché. 2012. Terminal transport of lytic granules to the immune synapse is mediated by the kinesin-1/Slp3/Rab27a complex. *Blood* 119: 3879–3889.
45. Bielska, E., M. Schuster, Y. Roger, A. Berepiki, D. M. Soanes, N. J. Talbot, and G. Steinberg. 2014. Hook is an adapter that coordinates kinesin-3 and dynein cargo attachment on early endosomes. *J. Cell Biol.* 204: 989–1007.
46. Kennedy, J. M., N. Fodil, S. Torre, S. E. Bongfen, J. F. Olivier, V. Leung, D. Langlais, C. Meunier, J. Berghout, P. Langat, et al. 2014. CCDC88B is a novel regulator of maturation and effector functions of T cells during pathological inflammation. *J. Exp. Med.* 211: 2519–2535.